Nuclear Inst. and Methods in Physics Research, A 943 (2019) 162490

Contents lists available at ScienceDirect

Nuclear Inst. and Methods in Physics Research, A

journal homepage: www.elsevier.com/locate/nima

Record fast-cycling accelerator magnet based on HTS conductor

Henryk Piekarz *, Steven Hays, Jamie Blowers, Brad Claypool, Vladimir Shiltsev

Fermi National Accelerator Laboratory, Batavia, IL 60510, USA

ARTICLE INFO

Keywords:
HTS conductor
Magnet
Accelerator

ABSTRACT

Four decades ago development of high-current superconducting NbTi wire cables revolutionized the magnet technology for energy frontier accelerators, such as Tevatron, RHIC and LHC. The NbTi based magnets offered advantage of much higher fields B and much lower electric wall plug power consumption if operated at 4.5 K but relatively small ramping rates dB/dt << 0.1 T/s. The need for the accelerators of high average beam power and high repetition rates have initiated studies of fast ramping SC magnets, but it was found the AC losses in the low-temperature superconductors preclude obtaining the rates in the excess of (1–4) T/s. Here we report the first application of high-temperature superconductor magnet technology with substantially lower AC losses and report record high ramping rates of 12 T/s achieved in a prototype dual-aperture accelerator magnet.

1. Motivation

Particle accelerators critically depend on development of high-field superconducting (SC) magnets [1–3] which allow to extend the energy reach and achieve desired cost and electric power efficiency of major physics facilities such as the Tevatron at Fermilab [4] – the pioneering machine operational from 1987 to 2011, the Relativistic Heavy Ion Collider [5] (RHIC, 1999 — now) at Brookhaven National Laboratory, and the Large Hadron Collider [6] (LHC) at CERN, Switzerland which operates since 2008. Note, that all these accelerators mostly operate in the regime of very slow beam energy ramp and their magnetic field ramping rates dB/dt are very low, 0.03–0.07 T/s. Next generation facilities such as muon colliders [7,8], future circular colliders [9,10] and high-intensity proton synchrotrons for neutrino research [11–13] accelerators demand substantially faster cycles of beam acceleration which in turn call for fast cycling accelerator magnets with dB/dt of the order of tens to hundreds of T/s. Normal conducting magnets can provide such rates – for example the JPARC 3 GeV proton rapid cycling synchrotron (RCS) magnets operate with dB/dt rates of 70 T/s [14] – but resistive power loss in the conductor and magnetization loss in the magnetic cores steel make them prohibitively power inefficient. Operation of the world's largest accelerator complex at CERN requires about 180 MW electric power and three smaller, low-energy normal conducting RCS's altogether boosting the proton energy beam from 50 MeV to 450 GeV consume just a little bit less electric power than much larger 6500 GeV SC LHC collider ring. Fast cycling SC magnets face great challenges due to the AC losses — energy dissipation in the conductor caused mostly by the magnetization of the superconducting filaments and due to coupling currents between the filaments in the strands. State-of-the-art cryogenic systems require 930 W of wall plug power to provide 1 W of cooling capacity for NbTi SC magnets at 1.8 K, and 230 W/W at 4.5 K [15] and that poses very stringent limits on the allowable AC losses in the low-temperature superconducting (LTS) magnet accelerators. To-date, the highest ramping rates achieved in the operational LTS accelerator magnets are about 4 T/s [16,17]. When comes to the accelerator magnet technology, the high temperature superconductors (HTS) [18] have triple advantage against the LTS based on the NbTi or Nb_3Sn superconductor– (i) much higher critical current densities and fields, (ii) lower AC losses with strands wide surface arrangement in a parallel orientation to the crossing magnetic field, and (iii) higher operational temperatures. In this paper we report the 12 T/s ramp rates achieved in a dual-bore accelerator HTS magnet prototype.

2. Rapid-cycling HTS accelerator magnet design

The AC losses in a SC magnet are proportional to the mass of the conductor and depend on total current I, frequency f, maximum field B, and temperature T. The physical mechanisms and scaling of the AC losses in the HTS tapes are different for the magnetization losses and for the transport-current losses as discussed in detail in [19,20]. Of importance for the magnet design is that the high current density of superconductors allows to strongly minimize the mass of the conductor and the exposure area to the magnetic field. For the HTS tape the critical current depends on both B-field strength and its orientation toward the tape axis. At the very low fields, however (e.g. < 0.1 T), the tape orientation toward magnetic field has only minor effect on the critical current.

* Corresponding author.
E-mail address: hpiekarz@fnal.gov (H. Piekarz).

https://doi.org/10.1016/j.nima.2019.162490
Received 18 March 2019; Received in revised form 18 June 2019; Accepted 30 July 2019
Available online 1 August 2019

For typical rapid cycling operation expected in future accelerators the inductive loss component due to self-fields induced by the AC transport current will dominate the AC power loss. The inductance L scales as N^2 with the number of turns and the minimal one can be achieved with a single-turn cable but for the required field B in the gap of the magnet very high current I conductor may be needed as $I \sim B/L^{1/2}$. For example, 2 T field has been achieved in the 20 mm dual-gap superferric DC magnet with 100 kA current in a NbTi-based single-turn power cable [21]. For the fast-cycling operation, the power supply voltage V grows with dI/dt and can be prohibitively large, therefore, to optimize technical feasibility and cost of such power supply some compromise between the magnet current and the magnet inductance is required. The rapid-cycling magnet design developed, tested and reported below — see Fig. 1- has three novel features: (a) it uses the high-current density HTS conductor, (b) the conductor is placed inside the steel core of the magnet such that the magnetic field in the conductor is minimal, and (c) its two vertically aligned beam gaps are energized by one conductor. The choice of 3-turn conductor allows to operate the magnet with three times lower current than needed in a single turn option for the same field in the gap:

$$B = \mu_0 I N / g \quad (1)$$

(here g is the gap size, μ_0 is magnetic permeability of the vacuum) at the expense of acceptable 9-fold increase of the inductance. In such arrangement – conceptually proposed in [9] – the magnetic fields in the upper and lower gaps are of the same value but of opposite polarities that makes it uniquely beneficial for simultaneous acceleration of two beams at once — either beams of opposite charge particles (e.g. electrons and positrons, positive and negative muons, protons and antiprotons) circulating in the same direction in each of the gaps, or two beams of the same particles circulating in opposite directions. Also of importance for the particle acceleration application is that in such design, the ever existing particle beam losses and decay products which have lower energy than the primary beams will be bent out and particle sent away from the HTS conductor, thus minimizing its highly undesirable heating and therefore greatly easing the requirements for the particle collimation and radiation protection systems [22].

The quench propagation velocity in the HTS superconductor is very slow and that makes the quench detection and protection difficult [18, 23]. Operation of the HTS conductor at the temperature much lower than the critical one allows efficient use of a temperature-based quench detection system. This is achieved by having the total cross-section of the HTS superconductor sufficiently large to carry the design transport current up to, e.g. 30 K. Therefore, at the operational temperature set to 5 K there is a wide quench safety margin of some 25 K. For example, according to Eq. (1), $B = 1$ T field in g = 40 mm gap can be achieved with the total transport current of $I \cdot N = 36$ kA that requires the superconductor cross-section of about 1 cm^2 for the 30 K operations. That surely will be more than enough to operate at 5 K. Fig. 2 shows the magnetic field simulation [24] for the 1 T in 40 mm gap magnetic core made of Fe3%Si laminations with the HTS conductor contained within 80 mm (v) × 10 mm (h) space, i.e. with 8 cm^2 conductor cross-section area determined mostly by the size of the cooling liquid helium conduit pipes which support the HTS strands. To keep the AC losses in the HTS conductor at minimum, the conductor is placed such that the B-field crossing cable space is less than 5% of the gap field B, i.e. less than 0.05 T. The hysteresis power loss in the superconductor scales mostly linearly with the dB/dt rate [25]. The power loss in the magnetic core and of the cable structure are dominated by the eddy currents and scale as $(dB/dt)^2$ and square of the thickness of these components [26]. With 100 μm laminations of the Fe3%Si prototype magnet core and 0.5 mm wall thickness of SS cooling helium conduit pipes, these resistive power losses are strongly minimized and are negligible for the dB/dt rate range of the test.

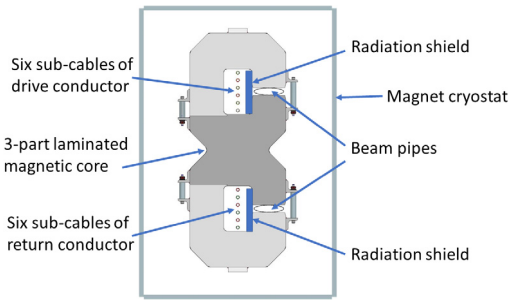

Fig. 1. Conceptual design of dual-bore HTS-based accelerator magnet.

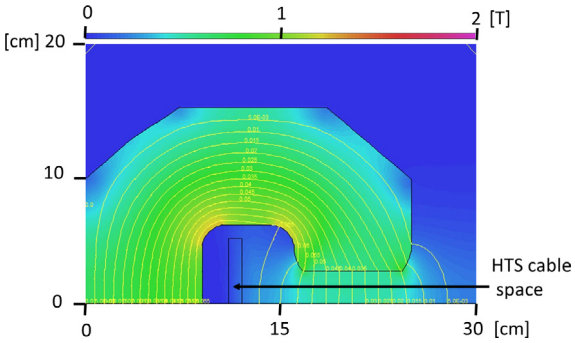

Fig. 2. Field simulation for 1 T magnet the 40 mm x 100 mm gap (quarter of the magnet shown).

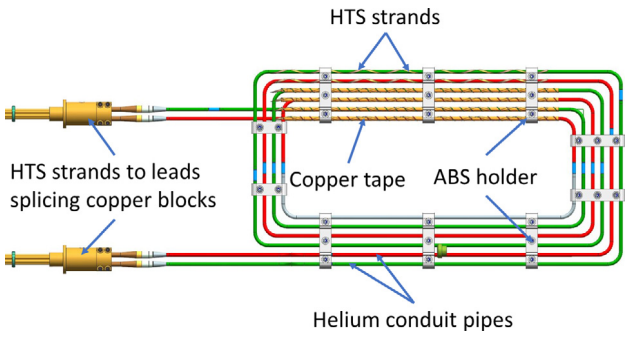

Fig. 3. Engineering design of the 3-turn HTS magnet coil.

3. Arrangement of HTS magnet test system

The 0.5 m long test magnet core of 620 mm × 255 mm cross-section is exactly of the shape shown in Fig. 1, with two beam gaps of 10 mm (height) × 100 mm (width). The 3-part core construction allows for simple assembly and installation of the HTS conductor coil. The full 3-turn conductor coil is shown in Fig. 3. The details of the HTS strands and copper tape windings are shown in Fig. 4. The 2 mm wide and 0.1 mm thick, HTS strands (Super-Power, Inc. [27]) are helically wound at 10 cm pitch on the surface of the helium conduit pipes made of 316LN stainless steel, 8 mm OD, 0.5 mm wall thickness. This arrangement makes ~1.05 mm averaged exposed width of a single HTS strand to the B-field. A single layer of the 0.1 mm thick, 12.5 mm wide oxygen-free high conductivity copper tape is wound helically over the strands to firmly secure their attachment to the cooling helium conduit pipe.

Up to 12 HTS strands can be placed on each helium pipe but for the test magnet there are only 2 strands attached to each conduit pipe. There are 12 strands in the magnet power cable of 24 m total length of which 12 m is inside the magnet core. The mechanical properties of

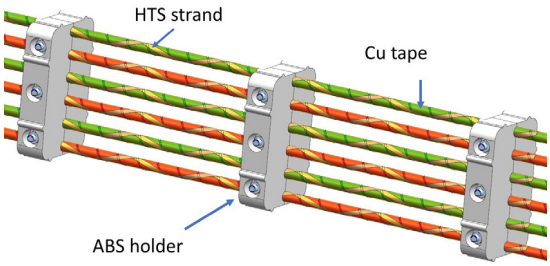

Fig. 4. Expanded view of the HTS coil section.

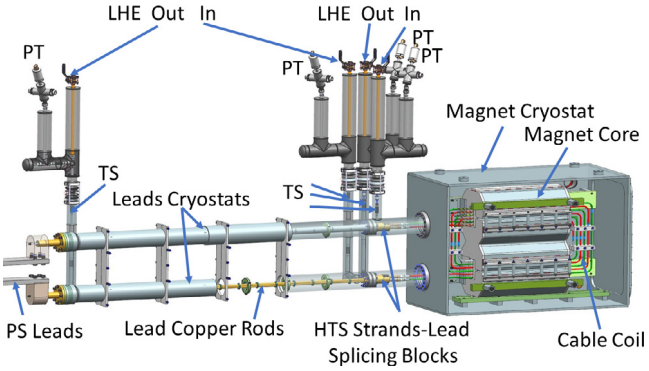

Fig. 5. HTS magnet test system arrangement. TS — temperature sensors. PT — pressure transducers.

Fig. 6. View of the HTS test magnet setup: 1 – magnet, 2 – current leads, 3 – power supply, 4 – cryogenics and power supply controls, 5 – cryogenics support.

the HTS cable within the magnet core space are listed in Table 1, and the test magnet electrical properties in Table 2. The projected critical current is 6 kA at 30 K. But lack of long-term stability of the supplied helium pressure has limited AC power supply operations to a maximum of $I = 2$ kA current to avoid the HTS conductor quench during the low helium pressure (~1 bar) and consequently high temperature > 40 K excursions.

The AC current source is constructed of three, 1.5 Volt switcher cells similar to those reported in [28], arranged in series to maximize the output current while minimizing the required voltage.

The test system arrangement is shown in Fig. 5, and the actual test setup in Fig. 6. The magnet HTS conductor coil and the conventional (copper) current leads are cooled using separate liquid helium flows. The pressure and temperature sensors are placed in the inlets and outlets of the helium cooling circuits. The liquid helium from the magnet coil and the current leads exits into the 3.6 kW pipe-type heaters which warm liquid helium to the room temperature before passing it into the flow meters and then returning under suction to the cryogenic plant. The difference in helium temperatures measured at the inlet and outlet

Table 1
HTS cable components within magnet space.

Cable component	Volume [m^3]	Mass [g]	Resistivity (5 K) [Ω-m]
HTS strands			
REBCO layer	$2.4\ 10^{-8}$	0.15	–
Hastelloy C-276	$12\ 10^{-7}$	10.7	$1.2\ 10^{-6}$
Cu cup	$9.5\ 10^{-7}$	8.6	$8\ 10^{-10}$
Ag cup	$9.5\ 10^{-8}$	1.0	$1\ 10^{-10}$
Total	$22.5\ 10^{-7}$	20.5	–
Strands support			
Cryogenic pipe	$73\ 10^{-6}$	569	$5\ 10^{-7}$
Copper tape	$15\ 10^{-6}$	107	$8\ 10^{-10}$
Total	$88\ 10^{-6}$	676	–

Table 2
Electrical properties of the test HTS magnet.

Cable critical current @ 6.5 K	6 kA
Cable critical current @ 30 K	2 kA
Magnet critical current @ 30 K	6 kA
Magnet maximum applied current	1.9 kA
Magnet maximum B-field	0.23 T
Magnet resistance @ 6.5 K with leads at RT	340 μΩ
Magnet resistance @ 6.5 K with cold leads	150 μΩ
Magnet inductance	~ 96 μH
Leads inductance	~ 4 μH

of the conductor helium conduit pipe together with measured helium pressure and flow rate were used to determine the cryogenic power loss through the change of helium enthalpy [29], $\Delta H = H$ (He out) – H (He in). The change in enthalpy equals the change of system energy which when combined with helium flow rate (F) gives the generated heat: Q [W] = ΔH (J/g) × F (g/s). The 6.5 K single-phase liquid helium system of 1.7 bar pressure and 1 g/s flow rate was used for conductor cooling. Although the Cernox temperature sensors [30] were calibrated with the precision of ±0.02 K the estimated inlet–outlet temperature readout uncertainty was ± 0.1 K.

4. Magnet power test results and discussion

As the result of the test, operating the AC power supply at the 20 Hz repetition rate with dI/dt = 38 kA/s current sine-wave, we obtained the dB/dt rate of 12 T/s in each of the magnet's two gaps — see Fig. 7. At such B-field cycling rate no measurable helium temperature rise in the conductor loop was observed, therefore with the temperature exposed sensors error of ±0.1 K we project the upper limit of about 0.8 W for the cryogenic power loss in the HTS magnet cable.

In our previous study [31], the cryogenic power loss for the cable constructed of 4.1 mm wide and 0.25 mm thick HTS strands exposed to the ramping external fields of dB/dt = (4–20) T/s at 6.5 K were reliably measured. Also measured for comparison were losses in the NbTi-based SC cable constructed to carry the same critical current. Fig. 8 presents the results for both LTS and HTS cables and clearly indicates significant advantage of the latter. The HTS-based cable data are for the strands with wide surface arranged approximately parallel to the magnetic field, aligned within the about ±4°. It turned out that the NbTi cable data matched well the AC loss projections. The data for the HTS-based cable show power losses significantly lower than those of the NbTi cable but exceeded projections by about a factor of two possibly due to the twisting of the HTS strands inside the cryogenic pipe caused by the magnetic force. Under the conditions of the previous and current tests – relatively low B-fields and dB/dt rates – the hysteresis AC power losses in the superconductors are dominant mechanisms, so one can use the previous test results to estimate expected losses in the test described above. As the conductor area (~$6\ 10^{-3}$ m^2) exposed to the vertically crossing B-field is about the same for both tests then using the ratio of the superconductor volumes (24 mm^3/192 mm^3) and ramping rates in the two tests (1.2 T/s vs. 12 T/s) one can tentatively project

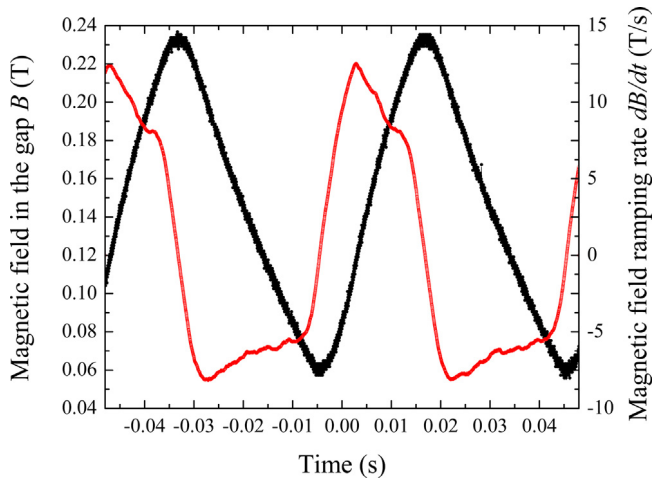

Fig. 7. Magnetic field B (black line, left vertical axis) and its ramping rate dB/dt (red line, right axis) in the HTS magnet gaps at 20 Hz.

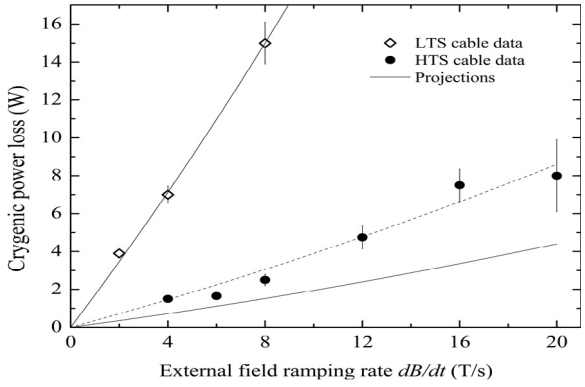

Fig. 8. Cryogenic power loss measured for LTS and HTS cables.
Source: Adapted from [31].

the cryogenic power loss to be about 0.06 W for the cable used in the current test, i.e., about an order of magnitude lower than the upper limit of 0.8 W obtained in this test.

We plan to improve the AC power supply system to energize the HTS-based prototype magnet in the dB/dt range from 20 T/s to 200 T/s which is required for e.g. future muon accelerators [7,8] and expect to be able to determine the AC power loss more accurately combining the cryogenic and electrical measurement methods [32,33].

5. Conclusion

We have developed the HTS-based fast cycling magnet suitable for a wide range of applications in high energy charged particle accelerators, have experimentally confirmed superiority of the HTS high-current conductors over traditional LTS ones in terms smaller AC losses in them, and finally, demonstrated the record high magnetic field ramping rates dB/dt of 12 T/s in the superconducting accelerator magnet prototype. Our results open new opportunities for the HTS magnet technology and for further developments toward required field quality, higher fields and other operationally critical properties of such magnets.

Authors would like to thank Frank McConologue for thoughtful engineering designs and Thomas Lynn for meticulous magnet assembly work. Fermilab is operated by Fermi Research Alliance, LLC under Contract No. DE-AC02-07CH11359 with the United States Department of Energy.

References

[1] M.N. Wilson, Superconducting Magnets, Oxford Science Publications, Oxford, 1983.
[2] K.H. Meß, P. Schmüser, S. Wolff, Superconducting Accelerator Magnets, World Scientific, Singapore, 1996.
[3] A. Asner, High Field Superconducting Magnets, Clarendon Press, Oxford, 1999.
[4] H. Edwards, Ann. Rev. Nucl. Part. Sci. 35 (1985) 605.
[5] M. Harrison, S. Peggs, T. Roser, Ann. Rev. Nucl. Part. Sci. 52 (1) (2002) 425.
[6] O. Brüning, P. Collier, Nature 448 (2007) 285.
[7] C. Ankenbrandt, et al., Phys. Rev. Spec. Top.-Accel. Beams 2 (8) (1999) 081001.
[8] D. Neuffer, V. Shiltsev, JINST 13 (2018) T10003.
[9] A. Milanese, H. Piekarz, L. Rossi, Proc. 5th Int. Part. Accel. Conf., Dresden, Germany, 2014, pp. 980–982.
[10] M. Benedikt, et al., Future Circular Collider. Vol. 2 : The Lepton Collider (FCC-ee), Report CERN-ACC-2018-0057 2018.
[11] H. Piekarz, Project X with Rapid Cycling and Dual Storage Superconducting Synchrotrons, e-print: arXiv:1205.1527.
[12] E. Prebys, et al., Proc. 7th Int. Part. Accel. Conf., Busan, Korea, 2016, pp. 1010–1012.
[13] S. Nagaitsev, V. Lebedev, A Cost-Effective Rapid-Cycling Synchrotron, e-print: arXiv:1812.10830.
[14] N. Tani, et al., IEEE Trans. Appl. Supercond. 14 (2) (2004) 409.
[15] S. Claudet, L. Tavian, P. Lebrun, G. Ferlin, U. Wagner, K. Brodzinkski, Energy efficiency of large cryogenic systems: the LHC case and beyond, Report CERN-ATS-2013-004 2013.
[16] A. Kovalenko, N. Agapov, H. Khodzhibagiyan, G. Moritz, Physica C 372 (2002) 1394.
[17] E. Fischer, et al., Proc. 3rd Int. Part. Accel. Conf., New Orleans, USA, 2012, pp. 3535–3537.
[18] Y. Iwasa, Cryogenics 43 (2003) 303.
[19] W.J. Carr Jr., AC Loss and Macroscopic Theory of Superconductors, CRC Press, 2014.
[20] C.M. Friend, in: A.V. Narlikar (Ed.), Studies of High Temperature Superconductors, Vol. 32, Nova Science Publishers, New York, 2000, pp. 1–61.
[21] H. Piekarz, et al., IEEE Trans. Appl. Supercond. 16 (2) (2006) 342.
[22] S. Redaelli, Beam Cleaning and Collimation Systems, e-print: arXiv:1608.03159.
[23] J. Paasi, J. Lehtonen, T. Kalliohaka, R. Mikkonen, Supercond. Sci. Technol. 13 (2000) 949.
[24] Dassault Systems, Opera Simulation Software; see https://operafea.com/ accessed February 26, 2019.
[25] M.D. Sumption, P.N. Barnes, E.W. Collings, Supercond. Sci. Technol. 18 (2005) 122.
[26] G. Moritz, Eddy currents in accelerator magnets, e-print: arXiv:1103.1800.
[27] SuperPower®2G HTS Wire Specifications, see http://www.superpower-inc.com/system/files/SP_2G+Wire+Spec+Sheet_2014_web_v1.pdf accessed February 11, 2019.
[28] S. Hays, B. Claypool, W. Foster, IEEE Trans. Appl. Supercond. 16 (2) (2006) 1626.
[29] A Heat Transfer Textbook, Third edition, Version 1.31 https://wiki.epfl.ch/./Lienhard-Lienhard_2008_A%20heat%20transfer%20textbook%252.accessed February 12, 2019.
[30] Cernox™Resistance Temperature Sensors for High Energy Physics Applications, see https://www.lakeshore.com/Documents/CernoxForHighEnergy.pdf; accessed February 11, 2019.
[31] H. Piekarz, S. Hays, J. Blowers, V. Shiltsev, IEEE Trans. Appl. Supercond. 22 (3) (2012) 5800105.
[32] K. Hatanaka, J. Nakagawa, M. Fukuda, T.Yorita, T. Saito, Y. Sakemi, T. Kawaguchi, K. Noda, Nucl. Instrum. Methods Phys. Res. A 616 (1) (2010) 16.
[33] B. de Bruyn, J. Jansen, E. Lomonova, Supercond. Sci. Technol. 30 (2017) 095006.